

Local orbital formulation of the Floquet theory of projectile electronic stopping

Marjan Famili,¹ Nicolò Forcellini ^{1,2} and Emilio Artacho ^{1,3,4}

¹*Theory of Condensed Matter, Cavendish Laboratory, University of Cambridge, J. J. Thomson avenue, Cambridge CB3 0HE, United Kingdom*

²*Beijing Academy of Quantum Information Sciences, Beijing 100193, China*

³*CIC Nanogune BRTA and DIPC, Tolosa Hiribidea 76, 20018 San Sebastián, Spain*

⁴*Ikerbasque, Basque Foundation for Science, 48011 Bilbao, Spain*



(Received 22 December 2021; revised 1 April 2022; accepted 9 May 2022; published 27 June 2022)

A recently proposed theoretical framework for the description of electronic quantum friction for constant-velocity nuclear projectiles traversing periodic crystals is here implemented using a local basis representation. The theory requires a change of reference frame to the projectile's, and a basis set transformation for the target basis functions to a "gliding basis" is presented, which is time-periodic but does not displace in space with respect to the projectile, allowing a local-basis Floquet impurity-scattering formalism to be used. It is illustrated for a one-dimensional single-band tight-binding model, as the simplest paradigmatic example, displaying the qualitative behavior of the formalism. The time-dependent nonorthogonality of the gliding basis requires care in the proper (simplest) definition of a local projectile perturbation. The Fermi level is tilted with a slope given by the projectile velocity, which complicates integration over occupied states. It is solved by a recurrent application of the Lippmann-Schwinger equation, in analogy with the previous nonequilibrium treatment of electron ballistic transport. Aiming towards a first-principles mean-field-like implementation, the final result is the time-periodic particle density in the region around the projectile, describing the stroboscopically stationary perturbation cloud around the projectile, out of which other quantities can be obtained, such as the electronic stopping power.

DOI: [10.1103/PhysRevB.105.245139](https://doi.org/10.1103/PhysRevB.105.245139)

I. INTRODUCTION

The study of energetic nuclei as projectiles shooting through matter has been of great interest for over a century [1,2]. An understanding of the emergent stopping phenomena (as the charged particles slow down in matter) from such processes is of significant applied interest in a variety of contexts, such as nuclear [3], aerospace [4], and medical [5]. It is also of fundamental interest, as a canonical problem of quantum systems strongly out of equilibrium.

Electronic stopping processes have been simulated over the years using various theoretical frameworks and approximations. From the theoretical side, there are two important paradigms for describing electronic stopping in the non-relativistic limit. Lindhard's linear response theory [6,7] is applicable to any host material and is accessible to first-principles theory [8]. However, it assumes weak effective interaction between the projectile and the target electrons, which is a very limiting approximation, especially at low velocities [9]. A fully nonlinear theory was proposed for the homogeneous electron liquid, including first-principles calculations, by Echenique, Nieminen, and Ritchie for the low projectile-velocity $v \rightarrow 0$ limit [10]. It was later extended to finite v [11–14], and it was also generalized to any (non-homogeneous) metal, still for the low- v limit [15]. Both the linear-response and jellium paradigms for electronic stopping assume a constant-velocity projectile. It is a very extended approximation in the community given the fact that the large projectile mass (as compared with the electronic) results in

a reduction of velocity which is barely appreciable in the nanoscale.

Explicit simulations of the electronic stopping processes using time-dependent tight-binding [9] and time-dependent density-functional theory (TDDFT) are the state-of-the-art techniques for the treatment of nonlinear stopping in materials beyond simple metals [16–34]. However, these calculations remain computationally expensive, since the projectile propagates across a large simulation box containing as much host material as possible, in periodic boundary conditions. In addition to guaranteeing convergence with system size (minimizing the effect of the multiple replicas of the projectile), these simulations rely on the heuristic ascertaining on having reached a stationary state.

A recent work introduced a theoretical framework which allows going beyond both the linear-response and jellium approximations in the direct characterization of the stationary state for the study of electronic stopping processes [35]. It is based on exploiting a discrete translational invariance in space-time for ion projectiles moving at constant velocity along periodic trajectories in crystals. When changing reference frame to the one moving with the projectile, the problem becomes time periodic and the theory can be formulated using Floquet theorem [36,37]. It becomes a time-periodic generalization of the time-independent problem faced when doing the same change of reference frame in jellium [10], now allowing for any periodic potential, and therefore any crystalline solid of whatever character and chemistry, no longer limited to ideal metals. The conservation of single-particle (Kohn-Sham

particle) energy in the scattering processes (in the projectile frame) in the jellium case now becomes Floquet quasienergy conservation [35].

A natural route towards a first-principles implementation of the Floquet theory of electronic stopping is using local functions as basis, for reasons analogous to those that gave very successful local-function implementations of electronic ballistic transport in the nanoscale [38–40], using scattering theory by the means of Green’s functions and Dyson’s equation. Here we propose the main conceptual ingredients for such an implementation of Floquet stopping theory, setting up the paradigm in terms of the simplest possible model: a one-band, one-dimensional (1D) tight-binding model, with a local perturbation moving at a constant velocity along the system, as established in Sec. III.

The first difficulty is encountered with the local functions of the basis moving past the projectile (at the origin) at a velocity of $-v$. This is addressed by introducing a “gliding” basis transformation to time-periodic but immobile (in space) functions (Sec. IV). The adequate description of a projectile local perturbation is presented in Sec. III B, and the Floquet scattering problem is then solved in a Green’s function formalism via the Dyson equation (Sec. V).

An independent-particle formalism is assumed, thinking of a mean-field-like implementation such as Kohn-Sham TDDFT. Single-particle occupation in this nonequilibrium setting is addressed in Sec. VI A. Finally, the time-periodic perturbed particle density $n(x, t)$ is obtained for the stationary solution around the projectile—actually, stroboscopically stationary: invariant when looking at it at times separated by the relevant time period.

The electronic stopping power S_e has been the key property in comparison with experiments, and it is also important for radiation-damage modeling at different length and time scales. It has been conventionally obtained from single-particle properties [10–14], namely, the scattering amplitudes and corresponding energy excitations for the individual scattering processes. Notwithstanding its being a remarkably successful approximation, obtaining the stopping power in terms of the force on the projectile appears as a more suitable definition, amenable to exact treatment under a wider scope of levels of theory. That force can be extracted from the particle density $n(x, t)$, as appears in Sec. VI B. Scattering amplitudes are also computed in the appendices.

II. THEORETICAL FRAMEWORK

Consider a projectile moving at constant velocity $\mathbf{v} = v\hat{\mathbf{v}}$ in the bulk of a crystalline solid. The constant-velocity projectile is a very extended assumption in most theoretical approaches to electronic stopping, in both linear and nonlinear response theories, albeit not all, since there is both theory and simulation work allowing for dynamical slowing down of the projectile (see, e.g., Ref. [41] for strongly coupled plasmas, or TDDFT simulations with Ehrenfest dynamics, as in references within Ref. [42]). Constant velocity breaks global energy conservation, the slowing down of the projectile of the real situation being captured by the energy uptake of the electrons to a good approximation for heavy projectiles. Following convention, we still call it the electronic stopping

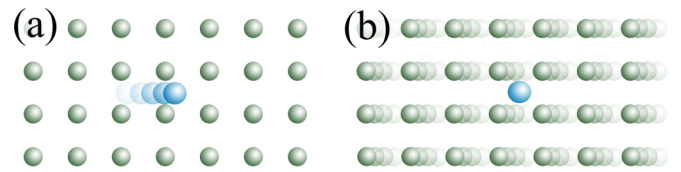


FIG. 1. Change of reference frame from the laboratory reference frame (LRF) (a) to the projectile reference frame (PRF), (b) results in a time periodic $H(\mathbf{r}, t)$ with period $\tau = a/v$, where a is the repetition length along the trajectory, and v is the projectile velocity.

problem and associated processes, in spite of the projectile not slowing down.

If the motion is along a spatially periodic trajectory of wavelength a , the group of discrete translations displacing simultaneously in space by na and in time by $-nv/a$, for any $n \in \mathbb{Z}$, leaves the Hamiltonian invariant. This symmetry in space-time can be exploited [35] through the application of the Galilean transformation $\mathcal{G} : \mathbf{r} = \mathbf{r}' - \mathbf{v}t$ [primed/unprimed indices indicating laboratory/projectile frame (LRF/PRF), respectively] putting the projectile at rest in the projectile frame. The Hamiltonian then takes the form

$$H(\mathbf{r}, t) = H_0(\mathbf{r} + \mathbf{v}t) + V_P(\mathbf{r}), \quad (1)$$

where H_0 is the Hamiltonian for the crystal structure in the PRF. We consider the crystal nuclei at crystalline ideal positions for the full consideration of the symmetry affecting the electrons, a widely used approach for exploiting Bloch’s theorem in electronic structure. $V_P(\mathbf{r})$ is a local scalar potential representing the (now static) projectile. Given the spatial periodicity a along the projectile trajectory, $H(\mathbf{r}, t)$ is time-periodic with period $\tau = a/v$. Fig. 1 illustrates the boost, showing how the target atoms move past the projectile. In a mean-field setting (such as KS-TDDFT), the projectile potential itself (now dressed with the Hartree, exchange and correlation components) can also depend on time, $V_P(\mathbf{r}, t)$. The key point, however, is that, if time-dependent at all, it will be generally expected to be time periodic in the long time limit, since it depends on the time-periodic perturbed density.

Following [35], the electronic stopping problem can then be addressed as a time-periodic scattering problem for the single-particle states. It represents a generalization to any velocity and any crystal structure of the nonlinear jellium theory of Ref. [10]. Its validity is obvious for noninteracting particles. For TDDFT this statement requires further support. It is known from the exact nonlinear theory in the limit of zero velocity [15] that the evaluation of the electronic stopping power S_e demands a dynamical exchange-correlation term in addition to the one coming from single-particle scattering events. On the other hand, the particle density $n(\mathbf{r}, t)$ as obtained directly from the solution of the effective single-particle KS-TDDFT problem (in this case a scattering problem) can be exact for the exact XC functional and proper consideration of the initial conditions [43]. In our statement, electronic stopping problem refers to the calculation of the fully nonlinear density response, as opposed to using single-particle scattering events for the calculation of S_e . The focus of this paper is on obtaining $n(\mathbf{r}, t)$. It can be further shown with ample generality that S_e can be obtained from the force acting on

the projectile, as a known functional of that density. This is discussed at certain length in general for Ehrenfest dynamics in, e.g., Refs. [44,45], and for the electronic stopping problem in particular in Ref. [46]. The full implementation of a Floquet TDDFT stopping theory with explicit calculation of S_e will be the focus of future work, which will also include the consideration of caveats already discussed for Floquet TDDFT in general [47]. In this work, we focus on setting up the key formalism on a simpler tight-binding model, which already illustrates key new concepts and perspectives.

Floquet's theorem in this context implies that there are time-dependent solutions of the form

$$\Lambda_{n\mathbf{k}}(\mathbf{r}, t) = e^{-i\varepsilon_n(\mathbf{k})t/\hbar} \Psi_{n\mathbf{k}}(\mathbf{r}, t), \quad (2)$$

which represent the stroboscopically stationary solutions, where $\Psi_{n\mathbf{k}}(\mathbf{r}, t) = \Psi_{n\mathbf{k}}(\mathbf{r}, t + \tau)$ are the Floquet *modes*, i.e., the eigenstates of the Floquet Hamiltonian $\mathcal{H} = H - i\hbar\partial_t$ ($\partial_t \equiv \partial/\partial t$). They are labeled by the quasimomentum \mathbf{k} of the incoming *unperturbed* Bloch state of the host crystal (which becomes Floquet-Bloch in the PRF) with energy $E_n(\mathbf{k})$ (n being the band index), and

$$\varepsilon_n(\mathbf{k}) = E_n(\mathbf{k}) - \hbar\mathbf{k} \cdot \mathbf{v} + mv^2/2 \quad (3)$$

is the corresponding Floquet quasienergy for a single electron of mass m .

As usual in scattering theory, the asymptotic form of the scattering Floquet modes can be expressed

$$\Psi_{n\mathbf{k}}(\mathbf{r}, t) \sim \psi_{n\mathbf{k}}(\mathbf{r}, t) + \sum_{m, \mathbf{k}_f} S_{n\mathbf{k}, m\mathbf{k}_f} \psi_{m\mathbf{k}_f}(\mathbf{r}, t), \quad (4)$$

where m , quasimomenta \mathbf{k}_f and scattering amplitudes $S_{n\mathbf{k}, m\mathbf{k}_f}$ are determined with scattering theory techniques, including quasienergy conservation and outgoing boundary conditions. Throughout the paper, we will use capital letters to distinguish the perturbed wavefunctions from the corresponding unperturbed ones, as in Eq. (4) above, where $\psi_{n\mathbf{k}}(\mathbf{r}, t + \tau) = \psi_{n\mathbf{k}}(\mathbf{r}, t)$ is the unperturbed Floquet-Bloch mode. For more details on the scattering theory for the Floquet-Bloch states, we refer the reader to Refs. [35,48].

III. MODEL

The practical implementation of the above theory based on a local basis set is tried out in the following. A simple tight-binding (TB) model in one dimension (1D) serves the purpose of presenting the key concepts and formalization needed, and it serves as a paradigmatic example of the qualitative physics of the problem. In particular, once the reference frame is changed to the projectile's, the local basis functions for the target, which are static in the LRF, are neither static nor time-periodic, but displace with velocity $-\mathbf{v}$, and as such, are not suitable for solving the Floquet scattering problem. To address this issue, we propose a basis set transformation to a set of time-periodic basis states (with the same period τ) in Sec. IV for the 1D model, which is introduced here first (for the generalization to 3D see Appendix A).

A. One-band moving tight-binding model

In the laboratory frame, with one atom per unit cell and one orbital per atom, the Hilbert space Ω' is spanned by the orthonormal basis set given by the functions

$$\phi'_\mu(x') = \phi'(x' - R'_\mu) = \langle x' | \phi'_\mu \rangle, \quad \mu \in \mathcal{Z},$$

i.e., atomic orbitals with shape $\phi'(x')$, centered at the lattice vectors $R'_\mu = \mu a$. Prime indices indicate objects in LRF as stated in Sec. II. Assuming only nearest-neighbor hopping of electrons (γ) between lattice sites and on-site energy of ε_0 , the Hamiltonian can be written as

$$H'_0 = \varepsilon_0 \sum_\mu |\phi'_\mu\rangle \langle \phi'_\mu| - \gamma \sum_\mu (|\phi'_\mu\rangle \langle \phi'_{\mu+1}| + \text{H.c.}), \quad (5)$$

with H.c. indicating the Hermitian conjugate. The eigenvalues and eigenstates of this time-independent Hamiltonian satisfying $H'_0 |\psi'_k\rangle = E(k) |\psi'_k\rangle$ are

$$E(k) = \varepsilon_0 - 2\gamma \cos(ka), \quad (6)$$

$$|\lambda'_k\rangle = \frac{1}{\sqrt{N}} \sum_\mu e^{ika\mu} |\phi'_\mu\rangle, \quad (7)$$

labelled by the crystal momentum k , conserved in the unperturbed model. N is the number of unit cells in periodic boundary conditions. The quantum number k is not primed, since it unequivocally labels the Bloch states in both LRF and PRF.

The Bloch waves in the real-space representation and with explicit time dependence in the energy phase,

$$\lambda'_k(x', t) = e^{-iE(k)t/\hbar} \frac{1}{\sqrt{N}} \sum_\mu e^{ika\mu} \phi'_\mu(x'), \quad (8)$$

can be transformed to the PRF via \mathcal{G} as [49]

$$\lambda_k(x, t) = e^{-i\frac{mv}{\hbar}x} e^{-i[E(k) + \frac{1}{2}mv^2]t/\hbar} \frac{1}{\sqrt{N}} \sum_\mu e^{ika\mu} \tilde{\phi}_\mu(x, t), \quad (9)$$

where the moving basis functions in PRF are defined as

$$\langle x | \tilde{\phi}_\mu(t) \rangle = \tilde{\phi}_\mu(x, t) \equiv \phi'_\mu(x + vt). \quad (10)$$

Note that in this frame the lattice, the crystalline potential, the basis functions and the electrons described by Bloch functions are all displacing with velocity $-v$. The Bloch waves transformed through \mathcal{G} have the Floquet form $\lambda_k(x, t) = e^{-i\varepsilon(k)t/\hbar} \psi_k(x, t)$, where $\psi_k(x, t)$ is the time-periodic Bloch-Floquet mode with quasienergy

$$\varepsilon(k) = E(k) - \hbar kv + mv^2/2. \quad (11)$$

The Bloch-Floquet modes can be immediately expressed by comparing Eq. (9) to the Floquet form, obtaining

$$\begin{aligned} \psi_k(x, t) &= e^{-ikvt} e^{-imvx/\hbar} \frac{1}{\sqrt{N}} \sum_\mu e^{i\mu ka} \tilde{\phi}_\mu(x, t) \\ &= e^{-ikvt} \frac{1}{\sqrt{N}} \sum_\mu e^{i\mu ka} \phi_\mu(x, t). \end{aligned} \quad (12)$$

In the above expression, the phase $e^{imvx/\hbar}$ was absorbed into the local basis $\phi(x, t)$, defining the new basis set as the set

defined by

$$\phi_\mu(x, t) = e^{-imvx/\hbar} \tilde{\phi}_\mu(x, t) \quad \forall \mu \in \mathcal{Z}. \quad (13)$$

The time-periodic function of Eq. (12) defines a Floquet mode, which is an eigenstate of the Floquet Hamiltonian $\mathcal{H}(x, t) = H(x, t) - i\hbar\partial_t$ with eigenvalues $\varepsilon(k)$ of Eq. (11), where $H_0(x, t)$ is the real-space representation of the TB Hamiltonian of Eq. (5), transformed into the moving frame. This is true by construction, but can also be explicitly verified (see Appendix B). This simple result is key to the solution of the Bloch-Floquet scattering problem: by knowing the unperturbed Bloch-Floquet modes, the allowed asymptotic states of the single-particle Bloch-Floquet states are known from the start, since they have to satisfy quasienergy conservation [35,48].

B. Projectile potential

The system to be studied is that of a constant velocity projectile moving along the 1D crystal. A simple tight-binding representation of such a potential in the LRF would be

$$V_p = \begin{cases} |\phi'_\mu\rangle \varepsilon_p \langle \phi'_\mu|, & t \in [\mu\tau, (\mu+1)\tau) \\ 0, & t \notin [\mu\tau, (\mu+1)\tau) \end{cases}, \quad (14)$$

which represents a constant on-site shift by ε_p on the site the projectile is on, for the duration of its passage, i.e., the period $\tau = a/v$, after which it shifts to the adjacent site on the right (left) if the projectile velocity v is positive (negative). An alternative procedure to define the projectile potential operator directly on the projectile reference frame is discussed below (in Sec. IV A).

IV. GLIDING BASIS

We have been able to state the Floquet modes of the unperturbed system in terms of the original tight-binding basis even though the basis functions are not periodic themselves. This was because we were using the Bloch functions directly, which are quite close to the Floquet modes. The scattering formalism used, will need a local basis when dealing with the Floquet modes for the total Hamiltonian and the local perturbation induced by the projectile. The fact that the individual basis functions pass by the projectile once, never to return, makes them quite inconvenient.

A straightforward solution to that problem is the relabelling of the basis functions every period, as

$$\xi_\mu(x, t) = \phi_{\mu+n}(x, t), \quad (15)$$

where we have defined n from $t = n\tau + \delta t$, and $\delta t = t \bmod \tau$. It can be also expressed as

$$\xi_\mu(x, t) = \phi_\mu(x, \delta t).$$

The ξ_μ basis functions are time-periodic with period τ , as intended, and are localized in space on the same lattice as the original one, but are now statically defined in the PRF. However, the time dependence is markedly discontinuous, with the basis function continuously moving leftwards (for $v > 0$) during a period, at the end of which it performs a sudden jump rightwards to start again. Such behavior will be

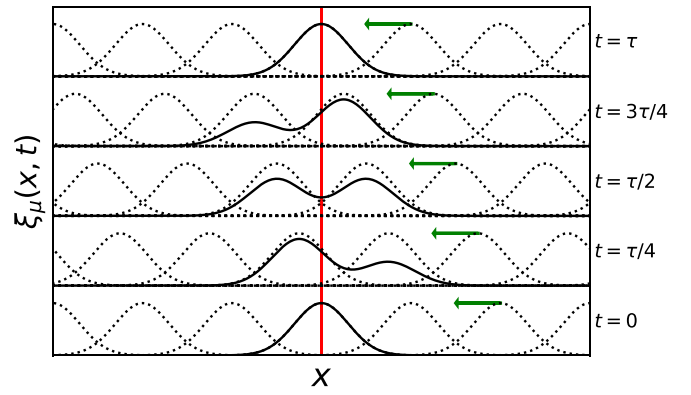


FIG. 2. Moving original tight-binding basis orbitals (dotted lines) and gliding basis function at site $\mu = 0$, for four time snapshots within a period. The red line indicates $x = 0$, the center of the projectile in the PRF.

hard to converge in the Fourier expansions to be performed below.

A transformation to a basis with smoother time dependence is proposed here for numerical convenience, each basis function gradually morphing onto its neighbor on the left (right) for $v > 0$ ($v < 0$), so that the label reassignment happens smoothly. Such procedure gives rise to the time-periodic, nonorthogonal gliding basis illustrated in Fig. 2, which is also defined on the static lattice in PRF, and which can be expressed as

$$\xi_\mu(x, t) = \mathcal{N}(t)[f(\delta t)\phi_{\mu+n}(x, t) + f(\delta t - \tau)\phi_{\mu+n+1}(x, t)] \quad (16)$$

for $\delta t \in [0, \tau]$, and $t = \delta t + n\tau$, and with

$$\mathcal{N}(t) = [|f(\delta t)|^2 + |f(\delta t - \tau)|^2]^{-1/2}$$

defined as the normalization at all times. It can also be written as

$$\xi_\mu(x, t) = \mathcal{N}(t)[f(\delta t)\phi_\mu(x, \delta t) + f(\delta t - \tau)\phi_{\mu+1}(x, \delta t)]. \quad (17)$$

The function $f(t)$ which defines the basis transformation, should be nonzero only in the $[-\tau, \tau]$ interval,

$$f(t) = \begin{cases} \tilde{f}(t), & t \in [-\tau, \tau) \\ 0, & t \notin [-\tau, \tau) \end{cases}.$$

Although it is not necessary, it is numerically convenient to ensure continuity (and hopefully smoothness) of the function at $t = \pm\tau$. Figure 2 illustrates the evolution of such a basis function. Note the use of $\phi(x, t)$ from Eq. (13) in this definition.

Since the basis given by the set $\{\xi_\mu(x, t), \forall \mu \in \mathcal{Z}\}$ spans the same space as spanned by $\{\phi_\mu(x, t), \forall \mu \in \mathcal{Z}\}$, converged results are independent of the gliding transformation used, the shape of $f(t)$ therefore representing a gauge freedom, which can be exploited for practical considerations such as maximising smoothness for Fourier transform truncation or simplicity in the equations. Examples of $\tilde{f}(t)$ can be found in Appendix C. The numerical calculations in this paper are done using the gauge function $\tilde{f}_2(t)$ in Eq. (C1), which ensures the continuity of the gauge function as well as of its first derivative, while the time-discontinuous transformation giving the

simplest formalism [of Eq. (15)] is given by the gauge step function of $\tilde{f}_4(t)$ in Eq. (C1).

A. Overlap and Hamiltonian in gliding basis

The gliding basis set $\{|\xi_\mu\rangle\}$ is nonorthogonal. Its overlap matrix, or metric tensor, $S_{\mu\nu} = \langle\xi_\mu(t)|\xi_\nu(t)\rangle$ is given by

$$S_{\mu\nu}(t) = \delta_{\mu\nu} + s(t) (\delta_{\mu,\nu+1} + \delta_{\mu,\nu-1}), \quad (18)$$

where we assumed that $f(t)$ is real, and defined $s(t)$ as

$$s(t) = \mathcal{N}(t)^2 f(\delta t) f(\delta t - \tau).$$

The unperturbed Hamiltonian in Eq. (5) can be expressed in the gliding basis when transferred to PRF. $H_0(t)$ is a tridiagonal matrix, with time-periodic sub- and supradiagonals, which annihilate after each period. The nonzero matrix elements are

$$\langle\xi_\mu, t|H_0|\xi_\mu, t\rangle = \varepsilon_0 - 2\gamma s(t),$$

$$\langle\xi_\mu, t|H_0|\xi_{\mu+1}, t\rangle = \langle\xi_\mu, t|H_0|\xi_{\mu-1}, t\rangle = \varepsilon_0 s(t) - \gamma,$$

and

$$\langle\xi_\mu, t|H_0|\xi_{\mu+2}, t\rangle = \langle\xi_\mu, t|H_0|\xi_{\mu-2}, t\rangle = -\gamma s(t),$$

although we will not need to solve for H_0 given that we already have the unperturbed (asymptotic) Floquet scattering modes from Eq. (12).

The projectile potential V_P of Eq. (14) becomes a matrix with elements

$$\begin{aligned} \langle\xi_0, t|V_P|\xi_0, t\rangle &= \varepsilon_p \mathcal{N}(t)^2 |f(\delta t)|^2, \\ \langle\xi_1, t|V_P|\xi_1, t\rangle &= \varepsilon_p \mathcal{N}(t)^2 |f(\delta t - \tau)|^2, \\ \langle\xi_0, t|V_P|\xi_1, t\rangle &= \varepsilon_p \mathcal{N}(t)^2 f(\delta t) f(\delta t - \tau), \\ \langle\xi_1, t|V_P|\xi_0, t\rangle &= \varepsilon_p \mathcal{N}(t)^2 f(\delta t) f(\delta t - \tau), \end{aligned} \quad (19)$$

and zero otherwise.

An alternative way of introducing the projectile potential is by parametrizing it directly in the gliding basis, already in PRF. It is appealing given its conceptual and implementation simplicity. The most straightforward choice would be to define V_P by specifying its representation in the gliding basis as the matrix

$$\langle\xi_\mu, t|V_P|\xi_\nu, t\rangle = \varepsilon_p \delta_{\mu\nu} \delta_{\mu 0}, \quad (20)$$

that is, a matrix with a constant on-site term at the zero site as the only nonzero term. This choice displays, however, two conceptual disadvantages: (i) V_P would then be gauge-dependent; a different choice of $f(t)$ in Eq. (16) not only affects convergence but also the results. (ii) Transforming back to the original basis, it can be shown that the decay length of the potential being represented depends on time, and actually diverges at $t = \tau/2$. It is shown in Appendix D.

Equation (20) can be expressed in operator form as

$$V_P = |\xi^0, t\rangle \varepsilon_p \langle\xi^0, t|,$$

where we are using the instantaneous dual basis $\{|\xi^\mu, t\rangle\}$, defined, as usual (see e.g. in this context [50]), as the set of

states (at any given time) that satisfy

$$\langle\xi^\mu|\xi_\nu\rangle = \langle\xi_\nu|\xi^\mu\rangle = \delta_\nu^\mu, \quad \forall \mu, \nu \in \mathcal{Z}.$$

It allows us to extend the proposal to alternative ones using locality in the natural and matrix representations of V_P [50], namely,

$$V_P = |\xi_0, t\rangle \varepsilon_p \langle\xi^0, t|$$

and

$$V_P = |\xi_0, t\rangle \varepsilon_p \langle\xi_0, t|, \quad (21)$$

respectively. The gauge-dependence problem remains for any of these choices, but the latter is not affected by the extreme time dependence of the range of the potential. It has the matrix form

$$\varepsilon_p \begin{pmatrix} s(t)^2 & s(t) & s(t)^2 \\ s(t) & 1 & s(t) \\ s(t)^2 & s(t) & s(t)^2 \end{pmatrix} \quad (22)$$

for the block for $\mu, \nu = -1, 0, 1$, being zero otherwise. For this paper, we choose to stay with the definition of V_P given by Eq. (19), given its gauge independence. Appendix D shows some results for the projectile defined as in Eq. (21) for comparison, using the gauge employed throughout this paper.

B. Floquet space

The space spanned by the moving basis set in Eq. (10), and equivalently, the one spanned by the gliding basis defined in Eq. (16), gives a Hilbert space at time t , $\Omega(t)$. As an object (for all times), it represents a curved manifold [50] that satisfies $\Omega(t + n\tau) = \Omega(t)$, even though the moving basis is not periodic. A Floquet space can be constructed as $\mathcal{F} = \Omega \otimes \mathcal{T}$. As geometrical object it would certainly deserve further mathematical attention, but, for the purposes of this work, the following suffices.

Consider any time-periodic function Φ spanned by the moving basis in the sense

$$|\Phi(t)\rangle = \sum_{\mu} \Phi^\mu(t) |\xi_\mu(t)\rangle. \quad (23)$$

Since both $|\psi(t)\rangle$ and all the $|\xi_\mu(t)\rangle$'s are periodic, then $\Phi^\mu(t)$ is periodic, too. These coefficients can therefore be expanded as

$$\Phi^\mu(t) = \sum_{m=-\infty}^{\infty} \Phi_m^\mu e^{im\omega t}$$

and we can re-express Eq. (23) as

$$|\Phi(t)\rangle = \sum_{\mu, m} \Phi_m^\mu e^{im\omega t} |\xi_\mu(t)\rangle. \quad (24)$$

This expression shows that the Floquet basis set $\{|\xi_\mu, m\rangle\}$, $\forall \mu, m \in \mathcal{Z}$ defined as

$$\langle\langle x, t | \xi_\mu, m \rangle\rangle = \xi_\mu(x, t) e^{im\omega t}, \quad (25)$$

constitutes a basis that spans the Floquet space \mathcal{F} corresponding to the original basis.

However, in our periodic case, time has become as space-like variable for the eigenproblem being faced for \mathcal{H} , the quasienergy ϵ becoming the conjugate of an auxiliary time t' in the so-called t, t' formalism [51], which allows for a generalization of the scattering formalism involving the Dyson equation in the extended Floquet space \mathcal{F} .

Knowing the exact eigenstates of H_0 , and therefore, the unperturbed Floquet-Bloch states of Eq. (31), the unperturbed retarded Green's function can be readily written as a matrix in \mathcal{F} as

$$g_{mm'}^{\mu\nu}(\epsilon) = \sum_k \frac{\langle \langle \xi^\mu, m | \psi_k \rangle \rangle \langle \langle \psi_k | \xi^\nu, m' \rangle \rangle}{\epsilon - \varepsilon(k) + i\eta}, \quad (33)$$

for $\eta \rightarrow 0^+$, or

$$g_{mm'}^{\mu\nu}(\epsilon) = \frac{1}{N} \sum_k \frac{\psi_{mk}^\mu \psi_{m'k}^{\nu*}}{\epsilon - \varepsilon(k) + i\eta}, \quad (34)$$

where

$$\psi_{mk}^\mu = \langle \langle \xi^\mu, m | \psi_k \rangle \rangle \quad (35)$$

are the expansion coefficients defined in Eq. (31).

The unperturbed density of states (DOS) $\rho^0(\epsilon)$ of the moving tight-binding chain is then obtained via

$$\rho^0(\epsilon) = -\frac{1}{\pi} \text{Im} \left[\sum_{mm'} \sum_{\mu\nu} g_{mm'}^{\mu\nu}(\epsilon) S_{\nu\mu, m'm} \right]. \quad (36)$$

Figure 3 shows $\rho^0(\epsilon)$ in the absence of a projectile where the lattice is moving with $v = -v_0$, with $v_0 = \gamma a/\hbar$. The DOS is periodically repeated in ϵ with a period of $\hbar\omega$, due to the structure of the quasienergy spectrum, as apparent for the Van Hove singularities appearing for Bloch states with a group velocity equal to the projectile's velocity v (zero velocity in PRF, see Fig. 3).

C. Projectile perturbation: Dyson equation

The effect of the projectile is obtained to all orders using the Dyson equation as for any scattering problem [52],

$$\mathbf{G}(\epsilon) = \mathbf{g}(\epsilon) + \mathbf{g}(\epsilon) \mathbf{V}_P \mathbf{G}(\epsilon) \quad (37)$$

as expressed as matrices in an abstract form, being $\mathbf{G}(\epsilon)$ the perturbed Green's function. It can be expressed in the computationally convenient way

$$\mathbf{G}(\epsilon) = [\mathbf{g}^{-1}(\epsilon) - \mathbf{V}_P]^{-1}, \quad (38)$$

which, given the structure of Eq. (37), can actually be solved as a matrix inversion of the matrix blocks corresponding to nonzero \mathbf{V}_P elements, which, from Eq. (19), correspond to two rungs of the ribbon in Fig. 3(a).

Hence, the perturbed density of states and the contributions from different basis functions can be calculated

$$\rho_{\mu m}(\epsilon) = -\frac{1}{\pi} \text{Im} \left[\sum_{\nu m'} G_{mm'}^{\mu\nu}(\epsilon) S_{\nu\mu, m'm} \right] \quad (39)$$

as a decomposition of the total density of perturbed states $\rho(\epsilon)$. The latter, suitably normalized, does not differ from $\rho^0(\epsilon)$, given the infinitesimal weight of the scattering region.

Hence, the decomposed functions are significant. Here we will use decomposition by site, showing

$$\rho_\mu(\epsilon) = \sum_m \rho_{\mu m}(\epsilon).$$

Equation (38) is solved by matrix inversion numerically and converged results are obtained for a cutoff $m_c = 50$, rendering matrices of 202×202 , given the two sites directly affected by the projectile potential in Eq. (19).

Figure 4 shows the perturbed DOS $\rho(\epsilon)$ projected on site $\mu = 0$ in the presence of the projectile introduced in Eq. (19) for a range of repulsive [Figs. 4(a) and 4(b)] and attractive [Figs. 4(c) and 4(d)] values of ε_P . They show how the spectral weight of regions of large $\rho^0(\epsilon)$ (in the region between the van Hove singularities) is shifted away, with peaks appearing in the low- $\rho^0(\epsilon)$ region. This is comparable to the localized state generated by a local perturbation in a static 1D TB chain (see Fig. 11 in Appendix E). For the moving system, however, a resonance appears instead of a localized state, given the fact that the unperturbed spectrum has no gaps.

It is apparent in Fig. 4 that the spectral weight shift upwards for the repulsive projectile potential is different from the equivalent shift downwards of the attractive counterpart, breaking the up-down symmetry that appears in the conventional locally perturbed TB (static) chain [52]. As illustrated in Appendix E, the static TB chain with a local perturbation also breaks that up-down symmetry whenever the perturbing potential breaks inversion symmetry (left-right symmetry in the chain): the usual picture of having $\rho_\mu(-\epsilon)$ for $\varepsilon_P > 0$ equal to $\rho_\mu(\epsilon)$ for $\varepsilon_P < 0$ and vice versa (for $\epsilon = 0$ in the middle of the TB band), does not hold when the perturbation is not centrosymmetric either around an atom or around the center of a bond. Therefore it is no surprise that we observe a similar effect in the case of the moving projectile, since the motion itself breaks that symmetry.

The site-projected perturbed DOS is expected to recover that of the unperturbed one when moving sufficiently far away from the projectile. This behavior is shown in Fig. 5, which displays $\rho_\mu(\epsilon)$ at various sites μ moving away from the projectile.

D. Projectile velocity dependence

Figure 6 shows the unperturbed and perturbed DOS of electronic stationary states for $\varepsilon_P = 0.7\gamma$, for various values of the projectile velocity, namely, $v = 0.5, 1.0, 2.0$, and 2.5 , in units of $v_0 \equiv \gamma a/\hbar$, along with the quasienergy bands of the unperturbed crystal. As before, the periodically repeated bands have an energy separation of $\hbar\omega = 2\pi\hbar v/a$, proportional to the velocity of the projectile.

For a velocity of $v = v_0$ [as in panels (d)–(f) of Figs. 6 and 4], there are quasienergies for which three asymptotic states are degenerate, allowing for, e.g., an electron coming in from the right to be transmitted (same state), scattered back towards the left or remain going to the right but more slowly (all in the PRF). For other values of the quasienergy (the region with lower $\rho^0(\epsilon)$) there is only one asymptotic state and there is no scattering channel beyond pure transmission: the projectile is transparent at those quasienergies. This is rather a peculiarity of the single band model, since any more realistic model

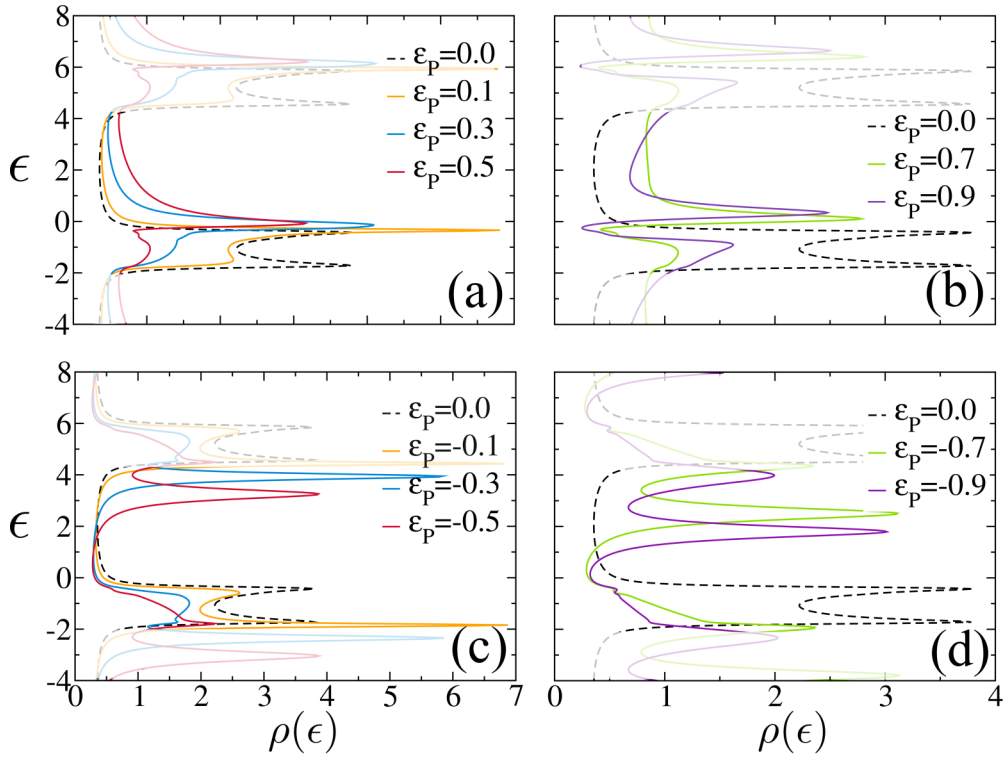


FIG. 4. Perturbed density of states (DOS) ρ vs quasienergy ϵ on site $\mu = 0$ for (a) repulsive weaker ($\epsilon_p = 0.1, 0.3,$ and 0.5 in units of hopping energy γ) and (b) stronger ($\epsilon_p = 0.7$ and 0.9) projectile potential. Same in (c) and (d) for attractive projectile potential. The unperturbed DOS is indicated by dashed lines. Faded region of the curves are for the replicas as in Fig. 3(b). The value of $\eta = 0.07\gamma$ is used throughout.

would include higher bands which would provide scattering options for any quasienergy and any projectile velocity.

Increasing the velocity from our $v = v_0$ starting value, the cell grows, the van Hove singularities enclosing the three-state regime get closer to each other, until, for v reaching the largest electronic group velocity (the Fermi velocity at half filling, $v_F = 2v_0$), both van Hove singularities merge into one.

Beyond that first critical velocity $v_1^c = v_F = 2v_0$ the projectile is swifter than any electron, the supersonic regime, and no scattering process takes place for any quasienergy, again, a peculiarity of the single-band model. An example is shown in Figs. 6(j)–6(l), for $v_p = 2.5\gamma a/\hbar$. The perturbed and unperturbed DOS locally differ, since the projectile potential still affects the wave functions locally, but there is no outgoing

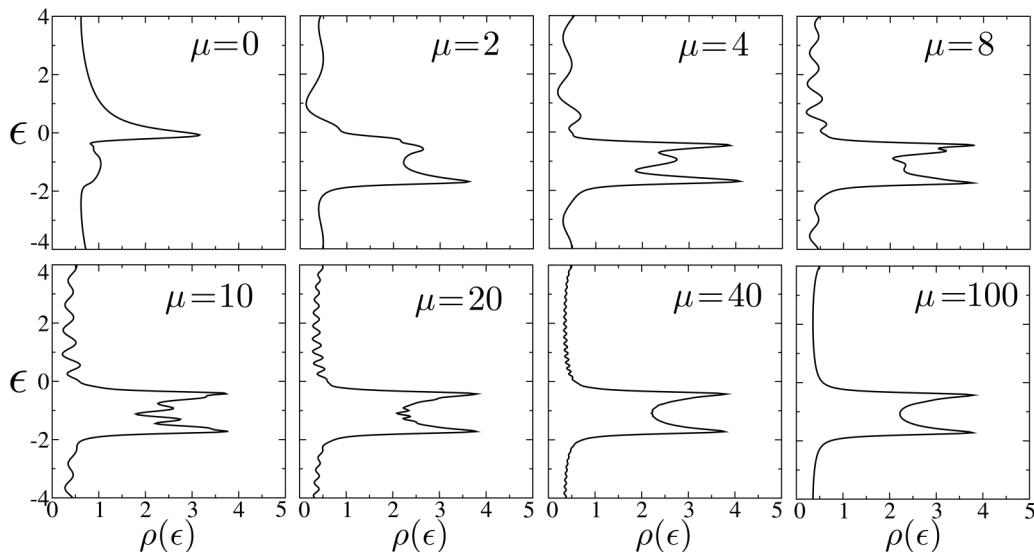


FIG. 5. Perturbed density of states ρ vs quasienergy ϵ evaluated at various sites μ moving away from the projectile (at $\mu = 0$).

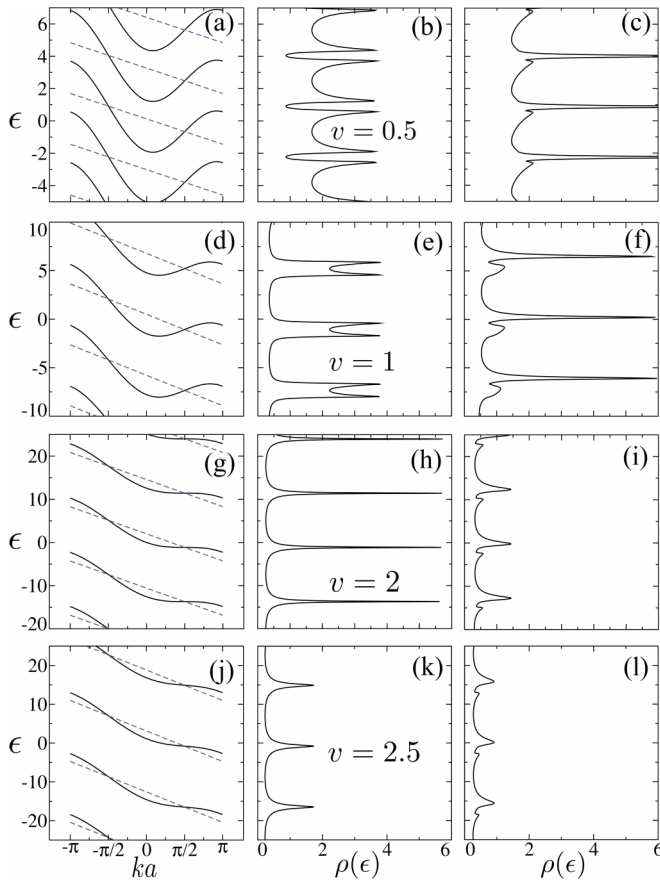


FIG. 6. Quasienergy bands of scattering states, unperturbed DOS and perturbed DOS for $v = 0.5$ [(a)–(c)], 1.0 [(d)–(f)], 2.0 [(g)–(i)], and 2.5 [(j)–(l)], all in units of $\gamma a/\hbar$. $v = v_F = 2\gamma a/\hbar$ is the highest group velocity of electronic states in the LRF, and the Fermi velocity at half-filling. v_p, v_F define the supersonic regime.

Bloch wave different from the incoming one regardless of which incoming one it is.

For slower projectiles, the quasienergy unit cell becomes smaller, the van Hove singularities of the unperturbed DOS get closer together squeezing the nonscattering region, thereby squeezing the resonance in the perturbed DOS with them, as illustrated in Figs. 6(a)–6(c). If for $v = v_0$ there were regions of quasienergy for which there were up to three compatible states, slowing down below a critical velocity, v_2^c , an interval of quasienergy values appear for which there are five degenerate asymptotic states, below v_3^c there are seven, and below v_n^c there are $2n + 1$, crowding towards the low-velocity limit, which becomes harder to treat, except for $v = 0$ strictly, which becomes the much simpler static impurity problem. It is a singular limit [53], analogous to the one found when treating low- k phonons in a crystal, which becomes hard when addressing the periodic superlattice capturing their long wavelengths, while it becomes trivial when strictly at the Γ point.

For velocity below $v_1^c = v_F$, the tilted bands of Fig. 3(b) display local minima and maxima. Further critical values v_n^c are defined by the velocities for which a horizontal line tangentially touches one minimum and one maximum (best seen as one single tilted band in an extended reciprocal space plot),

which happens when

$$\begin{aligned} v_F \cos ka &= [(n + 1/2)\pi - ka]v, \\ v_F \sin ka &= v. \end{aligned}$$

Solving for k and v yields

$$v_n^c = v_F \left\{ 1, 0.219, 0.129, \dots, \sim \frac{1}{(n + 1/2)\pi} \right\}$$

for $n \geq 1$ (the last expression being for large n).

VI. PARTICLE DENSITY

The independent-particle problem discussed so far can then be used to address the many-particle problem using a mean-field approach. The most attractive proposition given its efficiency and success in other contexts would be the one based on Kohn-Sham (KS) time-dependent DFT [43,54]. It has been shown, however, that Floquet TDDFT may be ill defined [47,55,56]. Nevertheless, the main experimental observable in the field of electronic stopping processes is the electronic stopping power, which relates to the suitable average of the force opposing the motion of the projectile, and which, as long as the projectile potential is local, can be obtained as the simple functional of the particle density $n(\mathbf{r}, t)$

$$\mathbf{F}_P(t) = - \int d^3\mathbf{r} n(\mathbf{r}, t) \nabla V_P(\mathbf{r}, t)$$

quite generally, regardless of the theory with which $n(\mathbf{r}, t)$ is obtained (see, e.g., the discussion of Ehrenfest forces in Ref. [44]). We will just assume it is a mean-field theory, and use the single-particle problem discussed in previous sections to define the perturbed particle density.

A. Occupation

Two extra ingredients are needed beyond what obtained so far, occupation and self-consistency. The latter is used to define the effective potential in the single-particle Hamiltonian iteratively from the perturbed density and/or perturbed wave-functions. However, in the context of this paper it only represents a redefinition of the parameters defining the model.

The occupation requires special attention. Occupation is normally quite trivially treated in equilibrium or near equilibrium, by simply integrating the relevant Green's functions from $-\infty$ to the Fermi level. However, in our case, occupied states are defined by the Fermi level in the LRF, which means that occupation in the PRF is defined by a “tilted Fermi level” (shown in Fig. 3). Therefore, it depends on the crystal momentum k of the unperturbed incoming scattering states. At any given quasienergy there can be both occupied and unoccupied states, as seen in Fig. 3.

We address the occupation problem analogously to earlier work for nonequilibrium ballistic transport [38], where equilibrium is defined separately in the two side electron reservoirs (leads), thereby having two separate Fermi levels. The idea is to obtain the scattered wave-functions from the Lippmann-Schwinger equation,

$$|\Psi_{n,k}\rangle = \{\mathbb{1} + \mathbf{G}[\varepsilon(k)]\mathbf{V}_P\}|\psi_{n,k}\rangle,$$

for all incoming scattering states that correspond to occupied states in the laboratory frame. We then use the scattered wave functions to build the occupied Green's function (equivalent to the “lesser” Green's function in Ref. [38]), as

$$\mathbf{G}^<(\epsilon) = \sum_k^{\text{occ}} \frac{|\Psi_k\rangle\langle\Psi_k|}{\epsilon - \epsilon(k) + i\eta}$$

the sum running over all perturbed states Ψ_k that result from the scattering of the initially occupied asymptotic (Bloch) states of the crystal. Integrated many-particle quantities such as the particle density are then obtained by suitable integrals of $\mathbf{G}^<(\epsilon)$ over all quasienergies. In our representation,

$$G_{mm'}^{<\mu\nu}(\epsilon) = \sum_k^{\text{occ}} \frac{\Psi_{mk}^\mu \Psi_{m'k}^{\nu*}}{\epsilon - \epsilon(k) + i\eta}.$$

The density matrix, $D_{mm'}^{\mu\nu}$, defined as

$$D_{mm'}^{\mu\nu} = \sum_k^{\text{occ}} \Psi_{mk}^\mu \Psi_{m'k}^{\nu*}, \quad (40)$$

can then be obtained from $\mathbf{G}^<$ by integrating over all quasienergies in one cell,

$$D_{mm'}^{\mu\nu} = -\frac{1}{\pi} \text{Im} \int^{\hbar\omega} G_{mm'}^{<\mu\nu}(\epsilon) d\epsilon,$$

from which the particle density is obtained directly (Sec. VI B), as well as properties depending on it, such as forces on atoms, and, from the force on the projectile, the electronic stopping power. It is illustrative, however, to see the density of occupied states projected on the different sites,

$$\rho_\mu^{\text{occ}}(\epsilon) = -\frac{1}{\pi} \text{Im} \left[\sum_{\nu mm'} G_{mm'}^{<\mu\nu}(\epsilon) S_{\nu\mu, m'm} \right], \quad (41)$$

which is equivalent to what displayed in Fig. 4, but now for $\mathbf{G}^<$, and it shown in Fig. 7.

B. Particle density $n(x, t)$

The particle density $n(x, t)$ of the 1D chain in the presence of the projectile in real space and time is given by

$$n(x, t) = \sum_{\mu\nu, mn} D_{mn}^{\mu\nu} \xi_\mu(x, t) \xi_\nu^*(x, t) e^{i(m-n)\omega t}, \quad (42)$$

where the $\xi_\mu(x, t)$ are the gliding basis functions as defined in Eq. (16).

The evolution of $n(x, t)$ during one time period (τ) is shown in Fig. 8 for various values of the perturbation potential. The time evolution is indicated by superimposing snapshots at $t = 0, \tau/5, 2\tau/5, 3\tau/5,$ and $4\tau/5$. Snapshots for subsequent times on the same sequence fall exactly on the depicted ones. The implicit orthonormal basis functions of the original TB model have been given an explicit shape (see Appendix G) for the plotting of $n(x, t)$.

The small wavelength oscillations depicted relate to the shape of orbitals, with the periodicity of the lattice, as can be seen in the absence of projectile, in panel (a) of Fig. 8. As ϵ_p is increased, a growing charge depletion is observed in the figure, around (and slightly in front of) the repulsive projectile

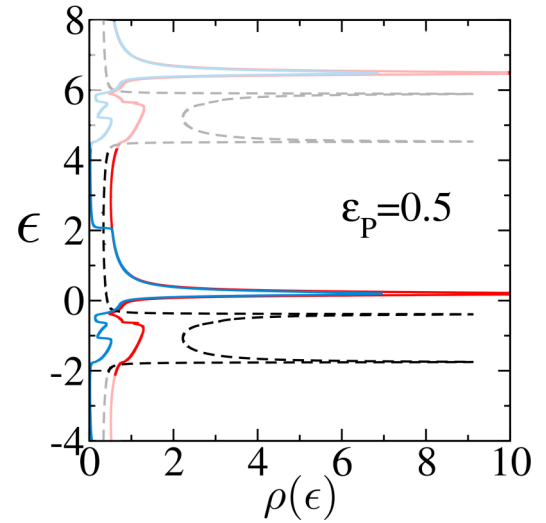


FIG. 7. Comparison between the unperturbed DOS (dashed black), perturbed DOS (red), and occupied perturbed DOS (blue) vs quasienergy ϵ in units of γ , for a projectile with velocity $v = v_0$ and perturbation potential $\epsilon_p = 0.5\gamma$ (with $\eta = 0.01\gamma$).

at $x = 0$. Since $v > 0$, the projectile is moving to the right, and it is also apparent how the density is enhanced on the right of the projectile and depleted on the left. The appearance of oscillations of larger wavelength than the lattice is also observed, in analogy with what happens in a static TB. A comparison with results for $v = 0$ is provided in Appendix E.

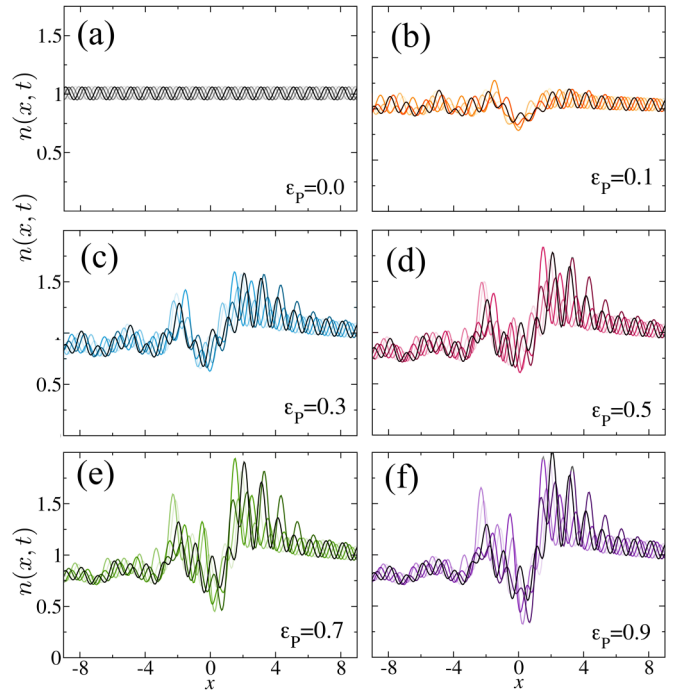


FIG. 8. Particle density $n(x, t)$ snapshots at $t = n\pi/5$ for $n = 0, 1, \dots, 4$ (lighter curves for earlier times), for a projectile of $\epsilon_p = 0, 0.1\gamma, 0.3\gamma, 0.5\gamma, 0.7\gamma,$ and 0.9γ (a) to (f), respectively. The velocity of the projectile is set to $v = v_0$.

VII. CONCLUSIONS

A local basis implementation of the Floquet theory of electronic stopping of Ref. [35] has been devised using a one-dimensional single-band tight-binding model for demonstration, but also as a simple (simplest) model for describing the stroboscopically stationary states resulting from electronic stopping processes for projectiles of any strength and velocity.

Once a gliding basis transformation is proposed to define a time-periodic but not displacing basis set in the projectile reference frame, the single-particle scattering states are obtained with a conventional Dyson-Green's functions scattering formalism. The integration over all incoming states for a determination of many-particle properties at a mean-field level is accomplished by summing over the perturbed scattering states from the occupied incoming ones using the Lippmann-Schwinger equation. From the Green's function for occupied states the density matrix and the particle density are readily obtained.

Although both the jellium work [10–14] and its Floquet generalization [35] offer expressions for the electronic stopping power as key magnitude in comparison with experiment, they are based on the individual single-particle scattering amplitudes and corresponding single-particle energy changes in the laboratory reference frame, which would be perfectly adequate for a system of truly noninteracting particles, but not for TDDFT (see, e.g., Ref. [15]) or similar mean-field theories. The quasienergy conserving individual Floquet scattering states of the Kohn-Sham particles give a good approximation to the particle density $n(x, t)$, however. The stopping power can then be obtained at the same level of theory directly from the force acting on the projectile, which is an explicitly known functional of the density [45] and which is straightforwardly calculated in any modern electronic structure program.

ACKNOWLEDGMENTS

We are very grateful for discussions with P. Ordejón, which helped with the parallel developments of our theory with those of nonequilibrium electronic ballistic transport, especially in the treatment of single-state occupations. Funding from the Leverhulme Trust is acknowledged, under Research Project Grant No. RPG-2018-254, as well as from the EU through the ElectronStopping Grant No. 333813, within the Marie-Sklodowska-Curie CIG program, and by the Research Executive Agency under the European Union's Horizon 2020 Research and Innovation programme (project ESC2RAD, Grant Agreement No. 776410). Funding from Spanish MINECO is also acknowledged, through Grant No. FIS2015-64886-C5-1-P, and from Spanish MICIN through Grant No. PID2019-107338RB-C61/AEI/DOI:10.13039/501100011033, as well as a María de Maeztu award to Nanogune, Grant CEX2020-001038-M funded by MCIN/AEI/10.13039/501100011033. A studentship funded by the Engineering and Physical Sciences Research Council of the United Kingdom, and Grants No. EP/L504920/1 and No. EP/N509620/1 are also acknowledged.

APPENDIX A: MOVING TIGHT-BINDING MODEL IN 3D

The Bloch basis are constructed starting from the set of local basis $\phi'_{li}(\mathbf{r}') \equiv \phi'_l(\mathbf{r}' - \mathbf{t}_i)$, where l indicates the orbital type and \mathbf{t}_i is a vector indicating the center of the atom in the primitive unit cell (position i). The Bloch basis can be then defined as

$$\chi'_{kli}(\mathbf{r}') = \frac{1}{\sqrt{N}} \sum_{\mathbf{R}'} e^{i\mathbf{k}\cdot\mathbf{R}'} \phi'_{li\mathbf{R}'}(\mathbf{r}'), \quad (\text{A1})$$

where the summation goes over all of the lattice vectors $\mathbf{R}' = \mu_1\mathbf{a}_1 + \mu_2\mathbf{a}_2 + \mu_3\mathbf{a}_3$ as $\phi'_{li\mathbf{R}'}(\mathbf{r}') = \phi'_l(\mathbf{r}' - \mathbf{t}_i - \mathbf{R}')$. They can be used as the basis for the single-particle eigenstates of the unperturbed crystal Hamiltonian

$$\lambda'_{nk}(\mathbf{r}') = \sum_{l,i} c_{nkli} \chi'_{kli}(\mathbf{r}') \quad (\text{A2})$$

and are associated with eigenvalues $E_n(\mathbf{k})$ for band n . Once the crystal states are found, they can be transformed to the PRF via the Galilean transformation \mathcal{G} as in the 1D case [49].

$$\lambda_{nk}(\mathbf{r}, t) = \sum_{l,i} c_{nkli} e^{-\frac{i}{\hbar}(E_n(\mathbf{k}) + \frac{1}{2}mv^2)t} e^{-\frac{i}{\hbar}m\mathbf{v}\cdot\mathbf{r}} \chi'_{kli}(\mathbf{r} + \mathbf{v}t). \quad (\text{A3})$$

The Bloch-Floquet modes are

$$\begin{aligned} \psi_{nk}(\mathbf{r}, t) &= e^{-i\mathbf{k}\cdot\mathbf{v}t} e^{-\frac{i}{\hbar}m\mathbf{v}\cdot\mathbf{r}} \sum_{il} c_{nkli} \chi'_{kli}(\mathbf{r} + \mathbf{v}t) \\ &= e^{-i\mathbf{k}\cdot\mathbf{v}t} e^{-\frac{i}{\hbar}m\mathbf{v}\cdot\mathbf{r}} \frac{1}{\sqrt{N}} \sum_{i\mathbf{R}} c_{nkli} e^{i\mathbf{k}\cdot\mathbf{R}} \tilde{\phi}'_{li\mathbf{R}}(\mathbf{r}, t), \end{aligned} \quad (\text{A4})$$

where Eq. (A1) was used and $\tilde{\phi}'_{li\mathbf{R}}(\mathbf{r}, t) \equiv \phi'_{li\mathbf{R}}(\mathbf{r} + \mathbf{v}t)$. Note that this expression is simply the generalization to 3D of the 1D Floquet modes of Eq. (12). It is, in principle, valid for any direction of $\mathbf{v} = v\hat{\mathbf{v}}$, and the resulting Floquet modes are time-periodic with a period $\tau = a/v$, being a the unit cell length of the crystal repetition along the projectile's trajectory, which depends on the relative disposition of the trajectory and the host's crystal structure. a can therefore take values from the length of the shortest lattice vector, all the way to infinity. The latter case will arise along incommensurate directions in the crystal, in which case the boosted Bloch states of Eq. (A4) are not strictly Floquet modes since they are not time periodic ($\tau \rightarrow \infty$).

The Floquet modes of Eq. (A4) are eigenstates of the Floquet operator $\mathcal{H}(\mathbf{r}, t) = H(\mathbf{r}, t) - i\hbar\partial_t$. Similarly, the localized gliding basis set (per orbital type) can be defined in the direction of the velocity

$$\begin{aligned} \xi_{li\mathbf{R}}(\mathbf{r}, t) &= \mathcal{N}(t)[f(\delta t)\phi_{li\mathbf{R}+na\hat{\mathbf{v}}}(x, t) \\ &\quad + f(\delta t - \tau)\phi_{li\mathbf{R}+(n+1)a\hat{\mathbf{v}}}(x, t)], \end{aligned} \quad (\text{A5})$$

where all the definitions from Sec. IV carry on unchanged. It should be noted that in 2D and 3D, other definitions for the gliding basis might be more convenient when considering velocity directions deviating from the primitive lattice vectors. In addition, depending on the exact direction of \mathbf{v} , the treatment can become numerically very complex—see the discussion in Ref. [48], p. 69, analogous to the $v \rightarrow 0$ limit (Sec. VD)—and other methods (or particularly tailored gauge choices) could be more suitable.

APPENDIX B: FLOQUET MODES FROM THE BLOCH STATES

Consider the moving Bloch state in the PRF

$$\lambda_k(x, t) = e^{-i\frac{mv}{\hbar}x} e^{-i[E(k) + \frac{1}{2}mv^2]t/\hbar} \sum_{\mu} \frac{e^{ika\mu}}{\sqrt{N}} \tilde{\phi}_{\mu}(x, t).$$

In the Bloch form, from Ref. [35],

$$\lambda_k(x, t) = e^{-i[E(k) + \frac{1}{2}mv^2 - \hbar kv]t/\hbar} [e^{ix(k-mv/\hbar)} u_k(x, t)],$$

where $u_k(x, t) \equiv u'_k(x + vt)$ is the periodic envelope of the Bloch eigenstate, thus defining the time-periodic mode $\psi_k(x, t)$ as the expression in brackets. By comparing the two expressions the Bloch-Floquet mode in this local basis representation is readily extracted

$$\psi_k(x, t) = e^{-ikvt} e^{-imvx/\hbar} \frac{1}{\sqrt{N}} \sum_{\mu} e^{i\mu ka} \tilde{\phi}_{\mu}(x, t),$$

periodic with the period of $\tau = a/v$ and eigenstate of the Floquet Hamiltonian $\mathcal{H}(x, t) = H(x, t) - i\hbar\partial_t$. Indeed, performing the direct calculation for $\psi_k(x, t)$ [using the simplified notation $f \equiv f(x, t)$]

$$-i\hbar\frac{\partial}{\partial t}\psi_k = -\hbar kv\psi_k + ve^{-i(kvt+mvx/\hbar)} \hat{p} \frac{1}{\sqrt{N}} \sum_{\mu} e^{i\mu ka} \tilde{\phi}_{\mu},$$

with $\hat{p} = -i\hbar\partial_x$. By applying the Hamiltonian transformed in the PRF $H(x, t) = H'(x, t) - v\hat{p} - mv^2/2$ to ψ_k [where $H'(x')$ is the Hamiltonian in the LRF, $x = x' - vt$ using our convention] one obtains

$$\begin{aligned} H\psi_k &= [E(k) + mv^2/2]\psi_k - ve^{-i(kvt+mvx/\hbar)} \hat{p} \frac{1}{\sqrt{N}} \\ &\times \sum_{\mu} e^{i\mu ka} \tilde{\phi}_{\mu}, \end{aligned}$$

with $E(k)$ being the energy of the Bloch state in the LRF. The above lead directly to the Floquet equation

$$\mathcal{H}(x, t)\psi_k(x, t) = \left[E(k) + \frac{1}{2}mv^2 - \hbar kv \right] \psi_k(x, t),$$

verifying explicitly that ψ_k is indeed the Floquet mode with the correct value for the quasienergy. The quasienergy replicas arise from the k values in the extended zone, since

$$\begin{aligned} k \rightarrow k + n\frac{2\pi}{a} &\Rightarrow \varepsilon(k) \rightarrow \varepsilon(k) - \hbar\left(n\frac{2\pi}{a}\right)v \\ &= \varepsilon(k) - n\hbar\omega. \end{aligned}$$

APPENDIX C: GAUGE FUNCTIONS FOR THE GLIDING BASIS

The function $f(t)$ defining the gliding basis transformation represents a gauge freedom that can be used for convenience. Here a few examples:

$$\begin{aligned} \tilde{f}_1(t) &= \left| \cos\left(\frac{\pi t}{2\tau}\right) \right|, \\ \tilde{f}_2(t) &= \cos^2\left(\frac{\pi t}{2\tau}\right), \end{aligned} \quad (\text{C1})$$

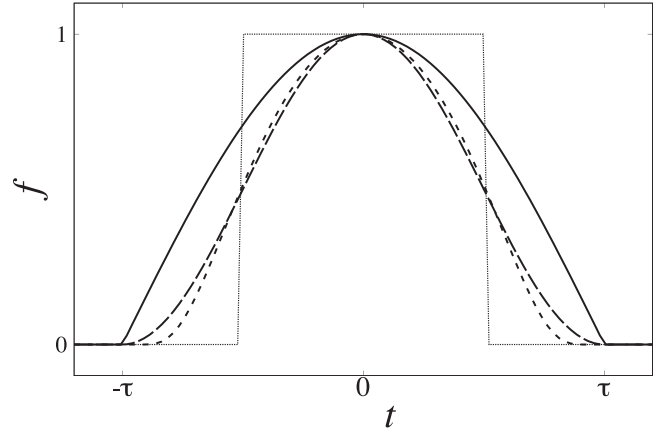


FIG. 9. Examples of gauge function $f(t)$, corresponding to the four in Eq. (C1), indicated by increasingly short dashes. $f_3(t)$ is depicted for $\alpha = 2$.

$$\tilde{f}_3(t) = e^{-\alpha t^2/(\tau^2 - t^2)},$$

$$\tilde{f}_4(t) = \Theta(t + \tau/2) - \Theta(t - \tau/2),$$

where $\Theta(t)$ is the Heaviside step function, and where $f(t)$ is defined from $\tilde{f}(t)$ as

$$f(t) = \begin{cases} \tilde{f}(t), & t \in [-\tau, \tau] \\ 0, & t \notin [-\tau, \tau] \end{cases}$$

The corresponding $f(t)$ functions are depicted in Fig. 9. $f_1(t)$ is convenient for simplicity, since $\mathcal{N}(t) = 1$ at all times, but shows a derivative discontinuity at $t = \pm\tau$, while $f_2(t)$ displays continuity of the function and first derivative, with a discontinuous curvature at $t = \pm\tau$. $f_3(t)$ has all derivatives continuous there, and contains the free α parameter that fattens the function within its limits. $f_4(t)$ gives the simplest, “relabelling” transformation, i.e., ξ orbitals follow the ϕ orbitals leftwise, but every period they abruptly jump by one lattice parameter rightwise. That is, $\xi_{\mu}(x, t) = \phi_{\mu}(x, \delta t - \tau/2)$. $f_2(t)$ is the one used in the calculations presented in this work.

As one would expect, the choice of gauge function should not make any difference in the physical quantities that are basis independent for a given Hilbert space. What can be different is the convergence behavior of such physical quantities when performing Fourier transformations with a cutoff. In Fig. 10, we show the difference in the convergence behavior of the total density of states when using gauge functions f_1 and f_2 , by computing the integral of the difference squared of the DOS's

$$\Delta\rho = \int [\rho^{f_1}(E) - \rho^{f_2}(E)]^2 dE \quad (\text{C2})$$

as obtained using gliding bases corresponding to f_1 and f_2 , for various cutoff thresholds m_c . Figure 10 clearly shows how the difference between the DOS computed using the two different gauge functions decreases as we increase the cutoff, and they eventually converge to the same function $\rho(E)$, as expected.

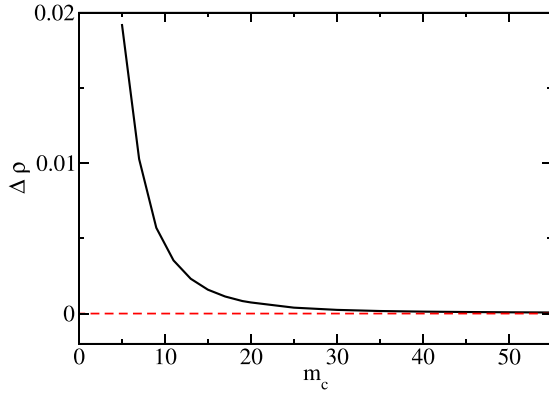


FIG. 10. Difference in convergence versus Fourier cutoff m_c of the total densities of states obtained by using the different gliding basis sets arising from gauge functions f_1 and f_2 . $\Delta\rho$ is as defined in Eq. (C2).

APPENDIX D: ALTERNATIVE PROJECTILES

If the projectile operator V_P is defined directly on the gliding basis (Sec. IV A), as, e.g.,

$$\langle \xi_\mu | V_P | \xi_\nu \rangle = \varepsilon_p \delta_{\mu\nu} \delta_{\mu 0},$$

knowing its form in the original basis requires the determination of the inverse of the basis transformation of Eq. (16).

1. Inverse transformation tensor

The basis set transformation in Eq. (16) can be expressed as

$$|\xi_\mu\rangle = |e_\sigma\rangle A_{\mu\sigma}^\sigma \quad (\text{D1})$$

assuming summation over repeated indices and dropping the time dependence for brevity.

$$A_{\mu\sigma}^\sigma = \langle e^\sigma | \xi_\mu \rangle$$

and $\{|e^\sigma\rangle, \forall \sigma = 1 \dots \mathcal{N}\}$ is the dual basis of $\{|e_\sigma\rangle\}$, such that $\langle e^\sigma | e_\delta \rangle = \langle e_\delta | e^\sigma \rangle = \delta_\delta^\sigma$, and, consequently, $|e^\sigma\rangle \langle e_\sigma| = |e_\sigma\rangle \langle e^\sigma| = P_\Omega$, the projector onto the subspace spanned by the basis. In this case

$$A_{\mu\sigma}^\sigma(t) = \mathcal{N}(t) [f(\delta t) \delta_{\mu+n}^\sigma + f(\delta t - \tau) \delta_{\mu+n+1}^\sigma]$$

which is a square matrix with a nonzero bidiagonal that displaces leftwards and downwards. For simplicity in the following, let us re-express it, for any given time, as

$$A_{\mu\sigma}^\sigma = c \delta_{\mu+n}^\sigma + s \delta_{\mu+n+1}^\sigma. \quad (\text{D2})$$

The inverse transform is defined as

$$|e_\sigma\rangle = |\xi_\mu\rangle B_{\sigma\mu}^\mu \quad (\text{D3})$$

with $B_{\sigma\mu}^\mu = \langle \xi^\mu | e_\sigma \rangle$. If both bases were orthonormal, the transformation matrix would be unitary, so that $B = A^{-1} = A^\dagger$. Since the gliding basis is not orthogonal, however, the inverse relations are $BA = AB = 1$ in the sense

$$A_{\mu\gamma}^\sigma B_{\gamma\nu}^\mu = \delta_\nu^\sigma \quad \text{and} \quad B_{\sigma\alpha}^\mu A_{\alpha\nu}^\sigma = \delta_\nu^\mu. \quad (\text{D4})$$

The sought expression for the original-basis representation of V_P depends on the inverse transformation, since we need

to express any $|e_\sigma\rangle$ in terms of the $|\xi_\mu\rangle$ states, and that is precisely Eq. (D3). Putting together Eqs. (D2) and (D4), we obtain

$$c B_{\sigma\mu}^\mu + s B_{\sigma-1\mu}^\mu = \delta_{\sigma\mu}^\mu,$$

and, again, for clarity, let us focus on $\mu = 0$ and call B_{σ}^0 as B_n , giving the recursive relation

$$c B_n + s B_{n-1} = \delta_n^0.$$

For $c > s$, the solution is

$$B_n = \begin{cases} 0 & n < 0 \\ \frac{1}{c} & n = 0, \\ \frac{1}{c} \left(-\frac{s}{c}\right)^n & n > 0 \end{cases},$$

whereas for $c < s$,

$$B_n = \begin{cases} \frac{1}{s} \left(-\frac{c}{s}\right)^n & n < -1 \\ \frac{1}{s} & n = -1. \\ 0 & n > -1 \end{cases}.$$

That is, the lower (upper) triangle of the infinite matrix is zero for $c > s$ ($c < s$), while the elements of the other triangle display a sign alternation when moving away from the diagonal, with an exponential decay of the magnitude,

$$|B_n| \propto e^{-\zeta n},$$

with $\zeta = \ln(c/s)$ for $c > s$ and $\zeta = \ln(s/c)$ for $c < s$. The decay length diverges when c approaches s , swapping triangle precisely at $c = s$. Since c and s represent a periodic function in time, one delayed with respect to the other, the B tensor starts diagonal, gradually extends into the upper triangle until full, then abruptly swaps into the full lower, which then gradually shrinks towards diagonal again (but shifted by one). And so it cycles.

2. Resulting projectile representation

The projectile potential expressed as $V_P = |\xi^0\rangle \varepsilon_p \langle \xi^0|$, becomes

$$V_{P,\sigma\lambda} = \langle e_\sigma | V_P | e_\lambda \rangle = \varepsilon_p B_{\sigma}^0{}^* B_{\lambda}^0$$

which gives a matrix with an exponential decay towards the lower-right quadrant and zero otherwise, the range then diverging as t approaches $n\tau$, and then swapping to the opposite upper-left quadrant.

This behavior is nonphysical and produces awkward behaviours. It is a rather unfortunate and nonintuitive consequence of establishing local decompositions in the nonorthogonal gliding transformation. However, remember that the alternative discontinuous-relabelling basis transformation

$$|\xi_\mu, t\rangle = |e_\mu, \delta t\rangle$$

is nothing by a particular choice of gauge function in the gliding transformation (a step function), and that the situation at mid-period is abrupt filling and swapping as well, although it may appear less explicitly.

The situation for the natural representation choice $V_P = |\xi_0\rangle \varepsilon_p \langle \xi_0|$ is less symmetric but ultimately suffering from the same oscillations in projectile-potential spatial range. This is why we have chosen to use the projectile as expressed in Eqs. (14) and (19).

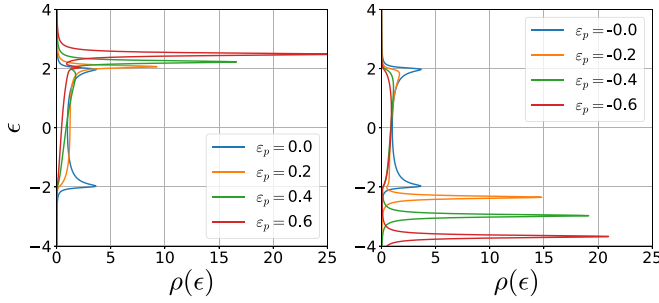


FIG. 11. Perturbed density of states ρ on site 0 vs energy ϵ , in units of γ , for a static single-band 1D tight-binding model with a perturbation potential of the form specified in Eq. (E1), for various values of ϵ_P (in units of γ) between 0.0 (black) and 0.6 (purple) on the left panel, and between 0.0 (black) to -0.6 (purple) on the right panel.

APPENDIX E: STATIC TIGHT-BINDING IMPURITY PROBLEM

For a better insight into features of the perturbed density of states of the Floquet scattering model, especially related to symmetry, the results of similar calculations for $v = 0$ are presented here, i.e., a local impurity in a 1D single-band static tight-binding model. A local on-site impurity perturbation of the form

$$V = |\phi_0\rangle\epsilon_P\langle\phi_0|$$

(LRF and PRF coincide for $v = 0$) is known to produce a bound state above (below) the band for positive (negative) ϵ_P , and a local density of states on the perturbed site $\rho_0(\epsilon)$ which becomes $\rho_0(-\epsilon)$ when changing the sign of ϵ_P , an “up-down” symmetry that is not observed in Fig. 4 of the Floquet model.

That up-down symmetry in the static model is very characteristic and related to the simplicity of the model, with a very exceptional up-down symmetry in the unperturbed density of states, plus the inversion symmetry in space implied by the defined impurity potential V . Indeed, that symmetry is still observed when introducing an off-diagonal V instead

$$V = (|\phi_0\rangle\gamma_P\langle\phi_1| + \text{H.c.})$$

(H.c. standing for Hermitian conjugate), or a combination of diagonal and nondiagonal (presenting the nonzero V matrix block, for sites 0 and 1)

$$V = \begin{pmatrix} \epsilon_P & \gamma_P \\ \gamma_P^* & \epsilon_P \end{pmatrix},$$

now preserving inversion symmetry around the center of the bond between sites 0 and 1.

However, the up-down symmetry disappears when the inversion symmetry is broken, which is simplest to describe with

$$V = \begin{pmatrix} \epsilon_{P0} & \gamma_P \\ \gamma_P^* & \epsilon_{P1} \end{pmatrix} = \epsilon_P \begin{pmatrix} 0.5 & 0.2 \\ 0.2 & 0.35 \end{pmatrix}, \quad (\text{E1})$$

where $\epsilon_{P0} \neq \epsilon_{P1}$, and where a set of particular values are proposed scaled by a single parameter ϵ_P . Figure 11 shows the perturbed density of states at site 0 for the specified per-

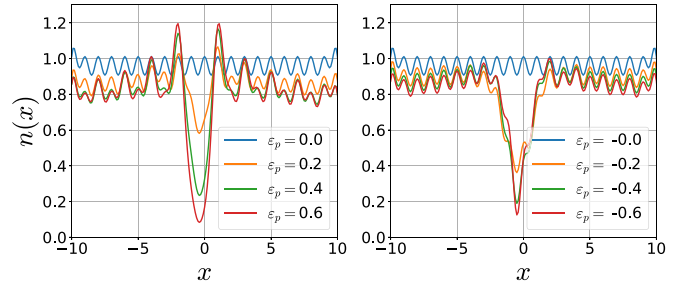


FIG. 12. Particle density $n(x)$ in real space for the same model and same values as Fig. 11. It has been obtained following the procedure using the Lippmann-Schwinger equation described in Sec. VIA, and therefore, it does not include the particle density associated to the bound state (note relevant only to the static attractive case).

turbation, for various values of the impurity potential strength ϵ_P . The up-down symmetry is visibly broken.

The analogous difference for attractive versus repulsive local perturbation for the Floquet model apparent in Fig. 4 relates to the same inversion symmetry breaking, although in the Floquet case it is due to the right to left motion of the crystal with respect to the projectile in the PRF.

The effect of the perturbing potential of Eq. (E1) on the particle density of the static chain is presented in Fig. 12 for a range of values of ϵ_P , repulsive on the left panel and attractive on the right. The functional form of the basis functions used for that plot is defined in Appendix G. The same particle density is shown over a longer range in real space in Fig. 13, showing the long-range perturbation characteristic in 1D.

APPENDIX F: ALTERNATIVE PROJECTILE DEFINITION

Figure 14 shows the same information as Fig. 4 but for the alternative definition of the projectile perturbing potential proposed in Eq. (21). It is defined directly on the gliding basis, which means that it is gauge-dependent, and, although convenient to write down, quite inconveniently dependent on the arbitrary choice of gauge, which is f_2 of Eq. (C1) in this case. The qualitative behavior is however unchanged.

APPENDIX G: LOCAL BASIS IN REAL SPACE

For the purpose of calculating the charge density in real space for producing Fig. 8, the real-space shape of the function $\phi(x)$ that gives rise to the original basis set of the

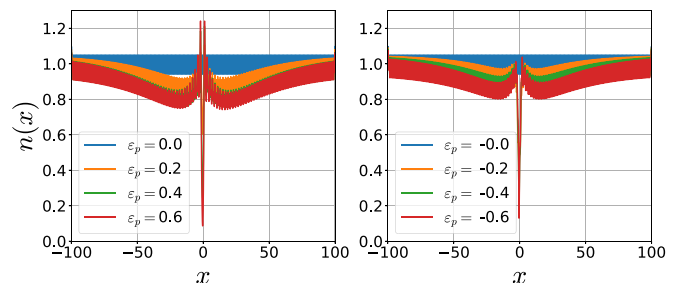


FIG. 13. Same as Fig. 12 over a longer range in real space.

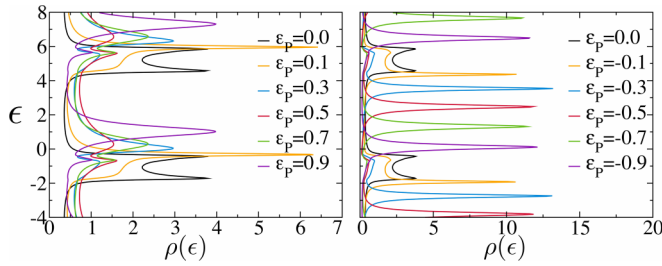


FIG. 14. Perturbed density of states ρ vs quasienergy ϵ for $v = v_0$, calculated using the alternative definition of the projectile potential as shown in Eq. (21), which is defined directly on the gliding basis, using the gauge specified as f_2 in Eq. (C1) in Appendix C. Left (right) panel shows DOS for several positive (negative) values of the perturbation potential strength ϵ_p .

tight-binding model $\{\phi_\mu, \mu \in Z\}$ has to be specified. It is defined as

$$\phi(x) = \mathcal{N} e^{-\alpha x^2} \cos\left(\frac{2\pi}{b}x\right),$$

where α defines the width of the Gaussian, and $\frac{2\pi}{b}$ originates an underlying oscillation that ensures (and b is chosen such) that the nearest-neighbor overlap is zero. For $\alpha \lesssim a$, the second nearest-neighbor overlap is not zero but negligible, giving an effectively orthonormal basis, once $\phi(x)$ is suitably normalized with

$$\mathcal{N} = \left(\frac{8\alpha}{\pi}\right)^{1/4} (1 + e^{-2\pi^2/\alpha b^2})^{-1/2}.$$

The values used in this work for Figs. 8, 12, and 13 are $\alpha = a$ and $b = 4a$.

APPENDIX H: SCATTERING AMPLITUDES

As argued in the paper, the safest way to obtain the electronic stopping power and characterize the electronic distortion is via the particle density, which is addressed in Sec. VIB. However, the single particle description can also render useful information for further analysis, such as excitation rates for the different single-particle excitation channels involved, as well as the traditional estimation of the stopping power directly from elementary processes and their single-particle energy jump in LRF, as used in Refs. [10,35]. The calculation of single-particle scattering amplitudes are presented here, from which such single-particle results can be extracted.

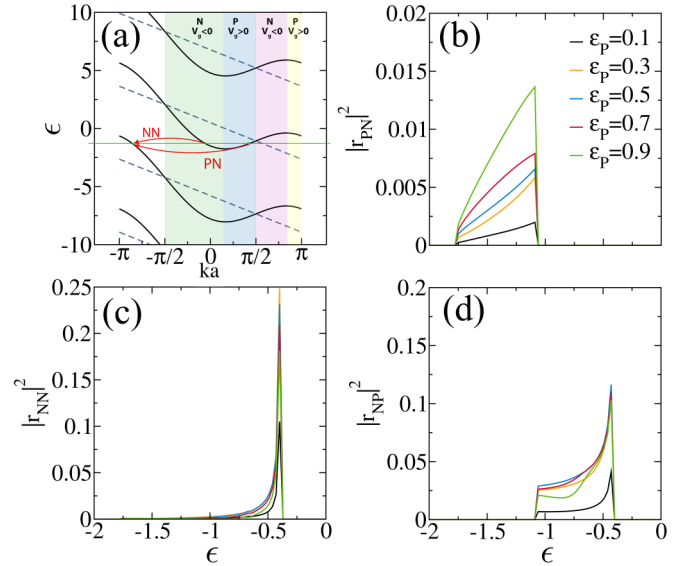


FIG. 15. Scattering matrix for $v = v_0$. (a) Schematic illustration for the labeling of the scattering probability coefficients, $|r_{ij}|^2$. Scattering coefficients: (b) $|r_{PN}|^2$ from states with $v_g > 0$ (right going states in the PRF, positive, P) to states with $v_g < 0$ (negative, N), (c) $|r_{NN}|^2$ with $v_g < 0$ to states with $v_g < 0$ and (d) $|r_{NP}|^2$ with $v_g < 0$ to states with $v_g > 0$, the three scattering possibilities beyond transmission for $v = v_0$, scattering from occupied states.

Starting from the transition operator or **T**-matrix for our model [57]

$$\mathbf{T}(\epsilon) = [\mathbf{V}_P + \mathbf{V}_P \mathbf{G}(\epsilon) \mathbf{V}_P], \quad (\text{H1})$$

the scattering matrix is then defined as

$$\mathbf{S} = \mathbb{1} - i \frac{a}{\hbar v_g} \mathbf{T}. \quad (\text{H2})$$

Scattering amplitudes have been calculated for $v = v_0$, for scattering from states with negative and positive (“N” and “P”) group velocities to states with the same quasienergy of negative and positive (“N” and “P”) group velocities, which are separately shown in Fig. 15. A visual aid for the labeling of the scattering amplitudes is depicted in Fig. 15(a). The magnitude of the scattering generally increases as the strength of the perturbation grows, as expected, although the situation is considerably richer than the customary 1D reflection and transmission coefficients, including the quite counter-intuitive behavior of perfect transparency for some incoming quasienergies regardless of the strength of the projectile perturbation.

[1] P. Sigmund, *Particle Penetration and Radiation Effects* (Springer International Publishing, Berlin, 2006)
 [2] P. Sigmund, *Particle Penetration and Radiation Effects* (Springer International Publishing, Berlin, 2014), Vol. 2.
 [3] R. E. Nightingale, *Nuclear Graphite* (Academic Press, London and New York, 1962).
 [4] M. Bagatin and S. Gerardin, *Ionizing Radiation Effects in Electronics: From Memories to Imagers* (CRC Press, Taylor and Francis, Boca Raton, Florida, 2016).

[5] W. P. Levin, H. Kooy, J. S. Loeffler, and T. F. DeLaney, *Br. J. Cancer* **93**, 849 (2005).
 [6] J. Lindhard, Kgl. Danske Videnskab. Selskab Mat.-Fys. Medd. **28** (1954).
 [7] J. Lindhard, M. Scharff, and H. E. Schiøtt, Kgl. Danske Videnskab. Selskab, Mat.-Fys. Medd. **33** (1963).
 [8] A. A. Shukri, F. Bruneval, and L. Reining, *Phys. Rev. B* **93**, 035128 (2016).

- [9] C. P. Race, D. R. Mason, M. W. Finnis, W. M. C. Foulkes, A. P. Horsfield, and A. P. Sutton, *Rep. Prog. Phys.* **73**, 116501 (2010).
- [10] P. Echenique, R. Nieminen, and R. Ritchie, *Solid State Commun.* **37**, 779 (1981).
- [11] K. Schönhammer, *Phys. Rev. B* **37**, 7735 (1988).
- [12] L. Böning and K. Schönhammer, *Phys. Rev. B* **39**, 7413 (1989).
- [13] E. Zaremba, A. Arnau, and P. Echenique, *Nucl. Instrum. Methods Phys. Res., Sect. B* **96**, 619 (1995).
- [14] A. F. Lifschitz and N. R. Arista, *Phys. Rev. A* **57**, 200 (1998).
- [15] V. U. Nazarov, J. M. Pitarke, C. S. Kim, and Y. Takada, *Phys. Rev. B* **71**, 121106(R) (2005).
- [16] J. M. Pruneda, D. Sánchez-Portal, A. Arnau, J. I. Juaristi, and E. Artacho, *Phys. Rev. Lett.* **99**, 235501 (2007).
- [17] A. V. Krasheninnikov, Y. Miyamoto, and D. Tománek, *Phys. Rev. Lett.* **99**, 016104 (2007).
- [18] M. Quijada, A. G. Borisov, I. Nagy, R. Diez Muiño, and P. M. Echenique, *Phys. Rev. A* **75**, 042902 (2007).
- [19] R. Hatcher, M. Beck, A. Tackett, and S. T. Pantelides, *Phys. Rev. Lett.* **100**, 103201 (2008).
- [20] A. A. Correa, J. Kohanoff, E. Artacho, D. Sánchez-Portal, and A. Caro, *Phys. Rev. Lett.* **108**, 213201 (2012).
- [21] M. A. Zeb, J. Kohanoff, D. Sánchez-Portal, A. Arnau, J. I. Juaristi, and E. Artacho, *Phys. Rev. Lett.* **108**, 225504 (2012).
- [22] M. A. Zeb, J. Kohanoff, D. Sánchez-Portal, and E. Artacho, *Nucl. Instrum. Methods Phys. Res., Sect. B* **303**, 59 (2013).
- [23] A. Ojanperä, A. V. Krasheninnikov, and M. Puska, *Phys. Rev. B* **89**, 035120 (2014).
- [24] R. Ullah, F. Corsetti, D. Sánchez-Portal, and E. Artacho, *Phys. Rev. B* **91**, 125203 (2015).
- [25] Li Weisen, Wang Xinwei, Zhang Xitong, Zhao Shijun, Duan Huiling, and Xue Jianming, *Sci. Rep.* **5**, 9935 (2015).
- [26] Z. Wang, S.-S. Li, and L.-W. Wang, *Phys. Rev. Lett.* **114**, 063004 (2015).
- [27] A. Schleife, Y. Kanai, and A. A. Correa, *Phys. Rev. B* **91**, 014306 (2015).
- [28] A. Lim, W. M. C. Foulkes, A. P. Horsfield, D. R. Mason, A. Schleife, E. W. Draeger, and A. A. Correa, *Phys. Rev. Lett.* **116**, 043201 (2016).
- [29] E. E. Quashie, B. C. Saha, and A. A. Correa, *Phys. Rev. B* **94**, 155403 (2016).
- [30] K. G. Reeves, Y. Yao, and Y. Kanai, *Phys. Rev. B* **94**, 041108(R) (2016).
- [31] C.-K. Li, F. Wang, B. Liao, X.-P. OuYang, and F.-S. Zhang, *Phys. Rev. B* **96**, 094301 (2017).
- [32] D. C. Yost, Y. Yao, and Y. Kanai, *Phys. Rev. B* **96**, 115134 (2017).
- [33] G. Bi, J. Kang, and L.-W. Wang, *Phys. Chem. Chem. Phys.* **19**, 9053 (2017).
- [34] R. Ullah, E. Artacho, and A. A. Correa, *Phys. Rev. Lett.* **121**, 116401 (2018).
- [35] N. Forcellini and E. Artacho, *Phys. Rev. Res.* **2**, 033151 (2020).
- [36] J. H. Shirley, *Phys. Rev.* **138**, B979 (1965).
- [37] P. Hanggi, *Driven Quantum Systems in Quantum Transport and Dissipation* (Wiley VCH, Weinheim, Germany, 1997).
- [38] M. Brandbyge, J.-L. Mozos, P. Ordejón, J. Taylor, and K. Stokbro, *Phys. Rev. B* **65**, 165401 (2002).
- [39] A. R. Rocha, V. M. García-Suárez, S. W. Bailey, C. J. Lambert, J. Ferrer, and S. Sanvito, *Nat. Mater.* **4**, 335 (2005).
- [40] J. Ferrer, C. J. Lambert, V. M. García-Suárez, D. Z. Manrique, D. Visontai, L. Oroszlany, R. Rodríguez-Ferradás, I. Grace, S. W. D. Bailey, K. Gillemot, H. Sadeghi, and L. A. Algharagholy, *New J. Phys.* **16**, 093029 (2014).
- [41] K. Morawetz and G. Röpke, *Phys. Rev. E* **54**, 4134 (1996).
- [42] A. A. Correa, *Comput. Mater. Sci.* **150**, 291 (2018).
- [43] M. Marques, A. Rubio, E. K. Gross, K. Burke, F. Nogueira, and C. A. Ullrich, *Time-Dependent Density Functional Theory*, Lecture Notes in Physics (Springer Science & Business Media, Springer, Berlin, 2006).
- [44] T. Todorov, *J. Phys.: Condens. Matter* **13**, 10125 (2001).
- [45] U. Saalmann and R. Schmidt, *Z. Phys. D: At. Mol. Clusters* **38**, 153 (1996).
- [46] J. F. K. Halliday, M. Famili, N. Forcellini, and E. Artacho, [arXiv:2203.15842](https://arxiv.org/abs/2203.15842).
- [47] N. T. Maitra and K. Burke, *Chem. Phys. Lett.* **359**, 237 (2002).
- [48] N. Forcellini, Floquet theory of electronic stopping processes of projectiles in solids, PhD thesis, University of Cambridge, 2020.
- [49] L. D. Landau and E. M. Lifshitz, *Quantum Mechanics: Non-Relativistic Theory*, 3rd ed. (Pergamon, New York, 2013).
- [50] E. Artacho and D. D. O'Regan, *Phys. Rev. B* **95**, 115155 (2017).
- [51] D. F. Martinez, *J. Phys. A: Math. Gen.* **36**, 9827 (2003).
- [52] E. N. Economou, *Green's Functions in Quantum Physics*, Springer Series in Solid State Science (Springer, Berlin, 1983).
- [53] M. Berry, *Phys. Today* **55**(5), 10 (2002).
- [54] E. Runge and E. K. U. Gross, *Phys. Rev. Lett.* **52**, 997 (1984).
- [55] P. Samal and M. K. Harbola, *Chem. Phys. Lett.* **433**, 204 (2006).
- [56] N. T. Maitra and K. Burke, *Chem. Phys. Lett.* **441**, 167 (2007).
- [57] M. S. Marinov and B. Segev, *J. Phys. A: Math. Gen.* **29**, 2839 (1996).